Journal of Industrial and Engineering Chemistry 113 (2022) 461–467

Contents lists available at ScienceDirect

Journal of Industrial and Engineering Chemistry

journal homepage: www.elsevier.com/locate/jiec

Tetraaryldiamine-based electron-transporting interlayers for performance and stability enhancement of organic solar cells

Alem Araya Meresa [1], Tae-won Lee [1], Solin Lee, Felix Sunjoo Kim *, Kwangyong Park *

School of Chemical Engineering and Materials Science, Chung-Ang University, Seoul 06974, Republic of Korea

ARTICLE INFO

Article history:
Received 4 May 2022
Revised 9 June 2022
Accepted 12 June 2022
Available online 18 June 2022

Keywords:
Tetraaryldiamine
Interfacial layer
Electron transport layer
Organic solar cell
Stability

ABSTRACT

Three novel tetraaryldiamines are synthesized and applied as an interlayer between zinc oxide (ZnO) and photoactive layers in PTB7-Th:$PC_{71}BM$ solar cells. The arylamines have an optical bandgap of 3.0–3.4 eV and do not interfere with the light-harvesting window of our polymer:fullerene combination. They enhance the power conversion efficiency from 7.48% in the control device to 8.95%, 8.18%, and 7.84% in PN-, PA-, and PAP-based devices, respectively. The dependence of photovoltaic parameters on the deposition conditions of the interlayer reveals that the current density and fill factor are the main parameters that increase when tetraaryldiamines are used as an interlayer. The external quantum efficiency increases from 73.1% in the bare ZnO device to 77.7–82.0% in the interlayer-incorporated devices. The power loss owing to the series and shunt resistances is reduced by a suitable alignment of the electronic energy levels with the interlayer and enhanced charge transfer through the components. Interlayer-incorporated devices also show a superior environmental stability compared to devices using bare ZnO. The results of this study should help advance the engineering strategies for organic solar cells with enhanced performances.

Introduction

Significant research effort has recently been focused on boosting the performance of organic solar cells via the design and synthesis of photoactive materials, charge-transporting layers, electrodes, and interlayers, as well as the optimization of device architecture [1–8]. The photoactive layer is typically wedged between the electron-transport layer and hole-transport layer. The transport layers and the electrodes are of extreme importance for the separation and extraction of charge carriers with minimal charge recombination in the cell, in order to boost the device performance [9–13]. Different materials, such as polymers, functionalized fullerene derivatives, polyelectrolytes, metal oxides and salts, and self-assembled monolayers, have been employed as electron-transporting layers [14–21]. Zinc oxide (ZnO) is widely used for an electron-transport layer, owing to its high transparency, appropriate electronic energy levels, and environment-friendliness [10,22]. However, ZnO also exhibits certain limitations, such as non-uniform morphology affecting its charge-transfer properties, surface defects acting as potential recombination sites, and the mismatch of surface energy with certain photoactive layers [22–26]. To overcome these drawbacks, passivation of ZnO by ionic liquids, self-assembled monolayers, polymers, and functionalized fullerenes has been proposed [27,28]. The deposition of thin buffer layers on a ZnO layer can smoothen the ZnO surface, improve the charge collection efficiency, and form a dipole moment at the interface to enhance charge transport [29,30]. Ideally, a suitable buffer layer exhibits solvent orthogonality with the active layer, charge-carrier selectivity with a suitable work function, and the ability to enhance device stability [31–33].

Recently, the performance of organic solar cells has been notably enhanced by employing amine-functionalized materials as an interlayer. For instance, an aliphatic amine derivative, called PDINN, was used as an interlayer in organic devices and reduced the work function of the metal cathode, thereby creating a better contact [34]. The use of a modified version of perylenediimides, called PDIN-H, as a cathode interlayer in organic solar cells with an inverted structure revealed an appreciable enhancement in device performance [35]. Generally, materials bearing amine groups are believed to reduce the work function of electroactive materials, including metals, polymers, and metal oxides [36]. This interesting feature motivated us to develop a series of arylamines and apply them as an interlayer sandwiched between the ZnO

* Corresponding authors.
E-mail addresses: fskim@cau.ac.kr (F.S. Kim), kypark@cau.ac.kr (K. Park).
[1] These authors contributed equally to this work.

https://doi.org/10.1016/j.jiec.2022.06.021
1226-086X/

and photoactive layers in organic solar cells with an inverted structure to enhance device performance and stability.

Herein, we report three tetraaryldiamines, namely *N,N,N′,N′*-tetrakis(4-(naphthalene-1-yl)phenyl)ethylenediamine (PN), *N,N,N′,N′*-tetrakis(4-(anthracene-9-yl)phenyl)ethylenediamine (PA), and *N,N,N′,N′*-tetrakis(4-(10-phenylanthracene-9-yl)phenyl)ethylene diamine (PAP), that were synthesized economically in higher yields via short synthetic routes from easily accessible reagents. The tetraarylamines are easy to handle using common organic solvents, and have a wide bandgap (≥3 eV) and an absorption in the ultraviolet region, allowing the harvesting of visible and infrared light at the photoactive layer. These arylamines were applied as an interlayer between a PTB7-Th:$PC_{71}BM$ photoactive layer and an electron-transporting ZnO layer in organic solar cells. The maximum power conversion efficiencies (PCEs) were 8.95%, 8.18%, and 7.84%, for the optimized ZnO/PN, ZnO/PA, and ZnO/PAP devices, respectively; these values were significantly higher than that of a control ZnO device (7.45%). The interlayer affected the short-circuit current density (J_{SC}) and fill factor (FF). A detailed investigation, conducted with the best-performing PN interlayer, revealed that the interlayer enhanced charge transfer through the layers and interfaces.

Experimental section

Materials

Naphthalene-1-boronic acid, 9-anthraceneboronic acid, (10-phenylanthracen-9-yl)boronic acid, chlorobenzene, butyl acetate, zinc acetate dehydrates, diiodooctane, silver (Ag), and molybdenum oxide (MoO_3) were purchased from Sigma-Aldrich. Tetrakis(triphenylphosphine)palladium(0), PTB7-Th (catalog name: PCE-10), $PC_{71}BM$, ethanolamine, and 2-methoxyethanol were purchased from Tokyo Chemical Industry (TCI), 1-Material, Nano-C, Daejung Chemicals & Metals, and Samchun Chemicals, respectively. An indium tin oxide (ITO; 10 Ω/sq)/glass substrate was purchased from AMG-Tech.

Synthesis

General procedure for preparation of tetraaryldiamines (3). *N,N,N′,N′*-Tetrakis(4-bromophenyl)ethylenediamine (**2**) was prepared according to the previous report [37,38]. To tetrakis(triphenylphosphine)palladium(0) (0.17 g, 0.15 mmol), arylboronic acid (3.23 mmol), and **2** (0.50 g, 0.74 mmol) in a two-neck round-bottom flask under nitrogen atmosphere, toluene (15.0 mL), ethanol (5.0 mL), and 2 M aqueous Na_2CO_3 solution (2.2 mL, 4.41 mmol) were added. The solution was heated at reflux for 72 h and cooled to room temperature. The reaction mixture was diluted with chloroform (100.0 mL), washed with water (×3) and brine, and dried over $MgSO_4$. The resulting solution was concentrated under vacuum to afford the crude product that was further purified by a column chromatography or a hot gravity filtration.

Preparation of *N,N,N′,N′*-tetrakis(4-(naphthalene-1-yl)phenyl)ethylenediamine (3a, PN). PN was prepared by the reaction of naphthalene-1-boronic acid (0.56 g, 3.23 mmol) and **2** (0.5 g, 0.74 mmol). The crude product was purified by column chromatography (CH_2Cl_2:*n*-hexane = 1:2) to afford **3a** (0.63 g, 96.4%) as a white powder: mp = 207–208 °C (uncorrected); TLC R_f 0.50 (CH_2Cl_2:*n*-hexane = 1:1); ^{1}H NMR (600 MHz, $CDCl_3$) δ8.03 (d, J = 8.35 Hz, 4H), 7.90 (d, J = 8.10 Hz, 4H), 7.84 (d, J = 8.14 Hz, 4H), 7.51 (dd, J_1 = 8.14 Hz, J_2 = 8.10 Hz, 4H), 7.47 (d, J = 8.58 Hz, 8H), 7.48–7.44 (m, 8H),7.39 (ddd, J_1 = 8.49 Hz, J_2 = 6.75 Hz, J_3 = 1.34 Hz, 4H), 7.27 (d, J = 8.58 Hz, 8H), 4.35 (s, 4H); ^{13}C NMR (150 MHz, CDCl3) δ 146.76, 139.87, 134.02, 133.88, 131.69, 131.14, 128.27, 127.35, 126.01, 125.95, 125.70, 125.43, 120.63, 50.09; HRMS (FAB, m/z) Calcd for $C_{66}H_{48}N_2$ [M + H]: 869.3896; found: 869.3904.

Preparation of *N,N,N′,N′*-tetrakis(4-(anthracene-9-yl)phenyl)ethylenediamine (3b, PA). PA was prepared by the reaction of anthracene-9-boronic acid (0.72 g, 3.23 mmol) and **2** (0.5 g, 0.74 mmol). The crude product was purified by column chromatography (CH_2Cl_2:*n*-hexane = 1:1) to afford **3b** (0.67 g, 79.6%) as a pale yellow powder: mp > 260 °C (uncorrected); TLC R_f 0.63 ($CHCl_3$:*n*-hexane = 3:2); ^{1}H NMR (600 MHz, CD_2Cl_2) δ 8.47 (s, 4H), 8.02 (br-d, J = 8.58 Hz, 8H), 7.83 (br-d, J = 8.88 Hz, 8H), 7.50 (d, J = 8.53 Hz, 8H), 7.43 (d, J = 8.53 Hz, 8H), 7.39 (ddd, J_1 = 8.58 Hz, J_2 = 6.47 Hz, J_3 = 1.05 Hz, 4H), 7.26 (ddd, J_1 = 8.85 Hz, J_2 = 6.47 Hz, J_3 = 1.22 Hz, 4H), 4.61 (s, 4H); ^{13}C NMR(150 MHz, $CDCl_3$) δ 146.98, 136.78, 132.46, 131.95, 131.41, 130.43, 128.30, 126.82, 126.38, 125.31, 125.04, 120.79, 50.09; HRMS (FAB, m/z) Calcd for $C_{82}H_{56}N_2$ [M + H]: 1069.4522; found: 1069.4537.

Preparation of *N,N,N′,N′*-tetrakis(4-(10-phenylanthracene-9-yl)phenyl)ethylenediamine (3c, PAP). PAP was prepared by the reaction of 10-phenylanthracene-9-boronic acid (0.96 g, 3.23 mmol) and **2** (0.5 g, 0.74 mmol). The crude product was purified by a hot gravity filtration (CH_2Cl_2:*n*-hexane = 1:4) to afford **3c** (0.39 g, 38%) as a pale brown powder: mp > 267 °C (uncorrected); TLC R_f 0.25 ($CHCl_3$:*n*-hexane = 1:1); ^{1}H NMR (600 MHz, $CDCl_3$) δ 7.92–7.88 (m, 8H), δ 7.69–7.65 (m, 8H), δ 7.62–7.57 (m, 8H), 7.57–7.50 (m, 20H), 7.50–7.45 (m, 8H) 7.31–7.25 (m, 16H), 4.63 (s, 4H); ^{13}C NMR(150 MHz, $CDCl_3$) δ 147.00, 139.10, 136.96, 136.88, 132.58, 132.28, 131.31, 130.13, 129.93, 128.37, 127.42, 126.96, 125.02, 124.99, 124.96, 120.88, 50.16.

Fabrication of organic solar cells.

Organic solar cells were fabricated on an ITO/glass substrate, and their structures are given as ITO/ZnO/tetraaryldiamine/PTB7-Th:$PC_{71}BM$/MoO_3/Ag. The ITO/glass substrate was washed with deionized water, acetone, and isopropanol, and treated with air plasma for 10 min. Zinc acetate dehydrates (1 g) and ethanolamine (0.28 g) in 2-methoxyethanol (10 mL) were mixed under vigorous stirring for 24 h in air [39]. The ZnO precursor solution was aged at room temperature for 1 day. After deposition of ZnO by spin-coating at 3 krpm for 40 s, the samples were annealed in air at 200 °C for 60 min to convert the precursor to a ZnO layer having a thickness of ∼ 44.8 nm. Tetraaryldiamines (PN, PA, and PAP) were dissolved in butyl acetate at designated concentrations (0.5, 1.0, 1.2, 1.5, and 2.0 mg/mL), stirred overnight at 50 °C, and deposited onto the ZnO layer by spin-coating at 3 krpm for 40 s, followed by annealing at 150 °C in ambient air for 10 min. The PTB7-Th:$PC_{71}BM$ (1:1.5 by weight ratio) blend was prepared in chlorobenzene with a total concentration of 25 mg/mL. A small amount (3 vol%) of diiodooctane was added in the polymer:fullerene blend as a processing additive. The blended solution was spun on the ZnO- and ZnO/arylamine-coated substrates at 800 rpm for 60 s; the resulting samples were transferred to a thermal evaporator to deposit MoO_3(10 nm) and Ag (100 nm) through a shadow mask under ultrahigh vacuum. The fabricated devices had active areas of either 4 or 9 mm^2. Photoactive layers were exposed to air without encapsulation before and after deposition of top electrode.

Characterization

A Varian VNS system was used for nuclear magnetic resonance (NMR) spectroscopic analysis (^{1}H NMR 600 MHz, ^{13}C NMR 150 MHz). Chemical shifts were reported in δ units (ppm) by assigning the tetramethylsilane resonance as 0.00 ppm in ^{1}H NMR and the $CDCl_3$ resonance as 77.2 ppm in ^{13}C NMR. Ultraviolet–visible (UV–vis) absorption spectra and photoluminescence

(PL) spectra were acquired using a V-670 spectrophotometer (JASCO) and a Cathodoluminescence Measurement System (PSI), respectively. Bandgaps of the synthesized tetraaryldiamines (PN, PA, and PAP) were determined from their solution UV–Vis spectra using the direct bandgap Tauc plot method [40]. Theoretical geometry optimization of the molecules and single-point energy calculation of their orbitals were performed based on density functional theory (DFT) at the B3LYP/6-31G(d) level of theory using the ORCA 4.2.1 package [41]. Melting point was measured using Barnstead Electrothermal 9100. A Keithley 2400 was used to measure the current–voltage curves. Ultraviolet photoelectron spectroscopy (UPS) was performed on the films using Sigma Probe (Thermo VG Scientific) equipped with a He I (21.22 eV) UV source. The energy scale was calibrated using a gold film as a reference. A PEC-L01 system (Peccell Technologies) was used to simulate the AM1.5G solar irradiation (100 mW/cm^2). Device measurements were carried out in ambient air at room temperature without any device encapsulation. Electrochemical impedance spectroscopy (EIS) analyses of the devices under 1-sun illumination were conducted in the frequency range from1 MHz to 20 Hz using a ZM2410 LCR meter with an AC voltage of 10 mV without any DC bias.

Results and discussion

The three tetraaryldiamines (PN, PA, and PAP) have a common flexible core of ethylene diamine and four π-conjugated arylene moieties connected to two nitrogen atoms. These arylamines were synthesized in high yields via an efficient synthetic path as depicted in Scheme 1. They are soluble in common organic solvents, including butyl acetate, tetrahydrofuran, toluene, and chloroform.

The tetraaryldiamines exhibited absorption profiles in the UV and blue regions of the spectrum (Fig. 1a). For PN, a strong absorption peak was observed at 333 nm. As the size of the aromatic moieties increased from naphthalene to anthracene, the absorption bands of the tetraaryldiamines exhibited a red-shift to 388 nm (PA). The attachment of a phenyl group to anthracene resulted in a further red-shift of absorption maximum wavelength to

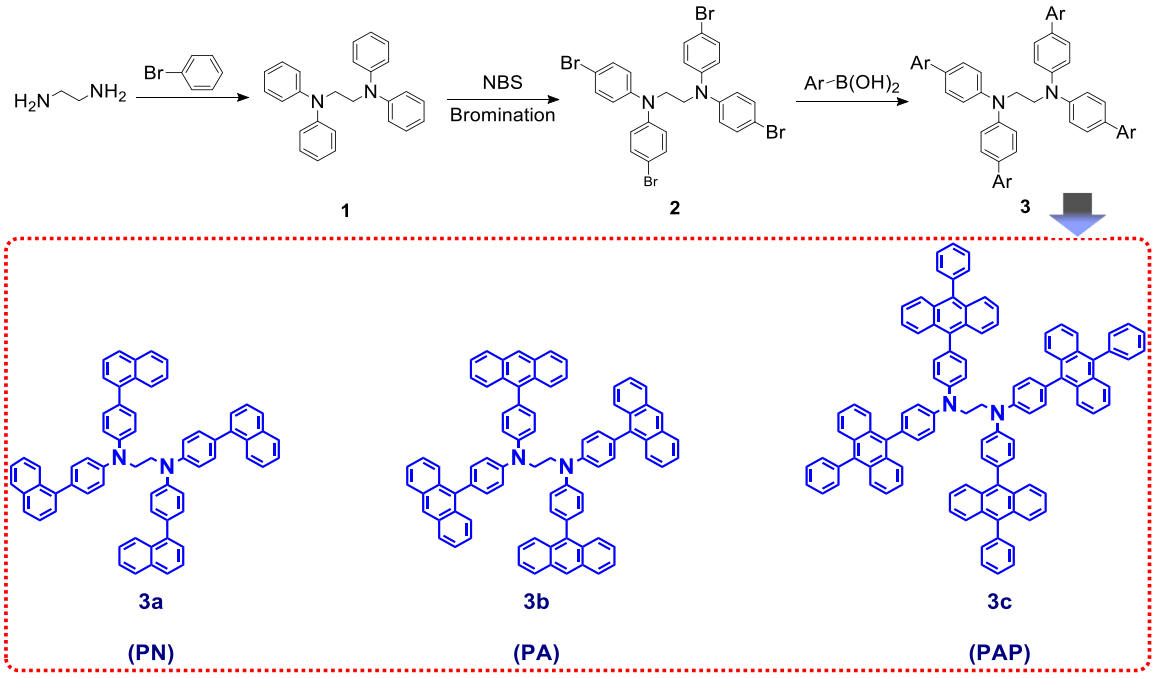

Scheme 1. Synthesis route of the tetraaryldiamines (PN, PA, and PAP).

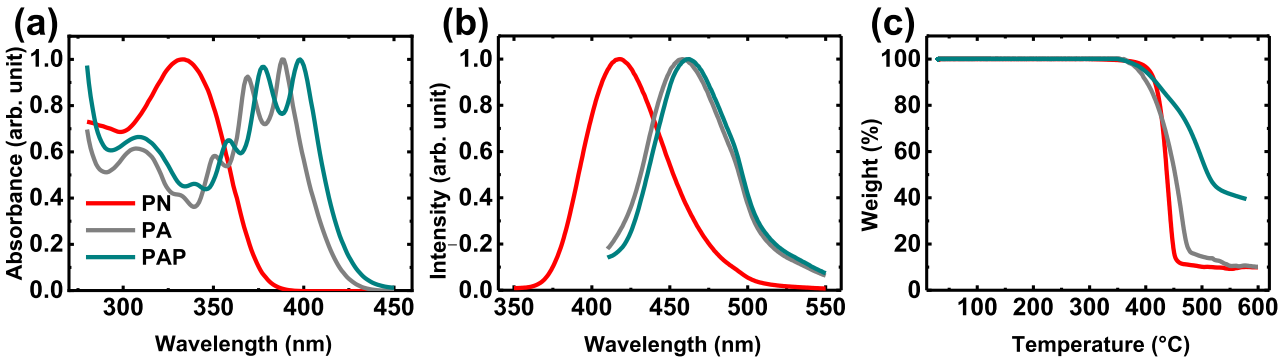

Fig. 1. Optical and thermal properties of PN, PA, and PAP: (a) UV–Vis absorption spectra, (b) PL spectra, and (c) TGA profiles.

398 nm (PAP). Similarly, the photoluminescence (PL) emission spectra of the three arylamines showed a significant red-shift of the peak as the conjugated unit became larger (Fig. 1b). Strong PL emissions of PN, PA, and PAP were observed at 418 nm, 459 nm, and 463 nm, respectively. Optical molecular bandgap, which was calculated from the UV–Vis absorption spectra using the Tauc method, showed a progressive decrease from 3.39 eV for PN to 3.05 eV for PA and to 2.99 eV for PAP. The trend in the optical bandgap was consistent with the DFT calculation results. The energy gap between the lowest unoccupied molecular orbitals (LUMOs) and the highest occupied molecular orbitals (HOMOs) narrowed from 3.90 eV (PN) to 3.33 eV (PA) and to 3.15 eV (PAP). The TGA data confirmed that the arylamines were thermally stable (Fig. 1c). The initial mass loss could be attributed to the decomposition of arylamines. The decomposition temperature ($T_{d,95\%}$) were 387 °C, 398 °C, and 406 °C for PA, PAP, and PN, respectively. The molecular properties are summarized in Table 1.

We applied the tetraaryldiamines (PN, PA, and PAP) as an electron-transporting interfacial layer in organic solar cells, which had the structure of ITO/ZnO/tetraaryldiamine/PTB7-Th:$PC_{71}BM$/MoO_3/Ag (Fig. 2). The energy levels of the constituent materials are suitable for the inverted structure [42]. Very smooth surface with a roughness of 0.9–1.2 nm was observed in both ITO/ZnO and ITO/ZnO/tetraaryldiamines (Fig. S7). The samples are denoted as ZnO/Px(y), where × represents the aromatic moiety (N, A, or AP) and y is its concentration (mg/mL). A preliminary study was conducted on the device to screen which arylamine was effective at what concentration in enhancing the performance of the solar cells (Fig. 2). A significant impact on the performance was observed for all arylamines to different degrees, which may originate from their common amine nature. Each material was tested by varying its concentration in butyl acetate and was found to perform optimally with the maximum PCEs of 8.95% for ZnO/PN(1.2), 8.18% for ZnO/PA(1.5), and 7.84% for ZnO/PAP(1.0). These PCEs are higher than that of the control sample without arylamines (7.48%). The photovoltaic parameters are listed in Table 2. In virtually all devices with the tetraaryldiamine interlayer, the short-circuit current density (J_{SC}) and the fill factor (FF) were significantly enhanced, leading to an enhanced PCE (Fig. 2b and Tables S1-S2). Because ZnO/tetraaryldiamine interlayers outperformed pristine ZnO and the arylamines shared structural similarities, we focused on PN as the model system of interest and conducted in-depth analyses.

To identify the major parameters of enhancement, we studied PTB7-Th:$PC_{71}BM$ solar cells fabricated with PN at various concentrations during interlayer deposition and characterized them under simulated AM1.5G solar irradiation at 100 mW/cm^2 (Fig. 3). The control device with pristine ZnO without an interlayer exhibited

Table 1
Molecular properties of tetraaryldiamines (PN, PA, and PAP).

Material	$\lambda_{Abs,Max}$ (nm)	λ_{Em} (nm)	E_g (eV)[a]	HOMO (eV)[b]	LUMO (eV)[b]	$T_{d,95\%}$ (℃)
PN	333	418	3.39	−5.00	−1.10	406
PA	388	459	3.05	−4.93	−1.60	387
PAP	398	463	2.99	−4.79	−1.64	398

[a] Calculated from the onset of absorption spectra in solution.
[b] Obtained from DFT calculations at the B3LYP/6-31G(d) level.

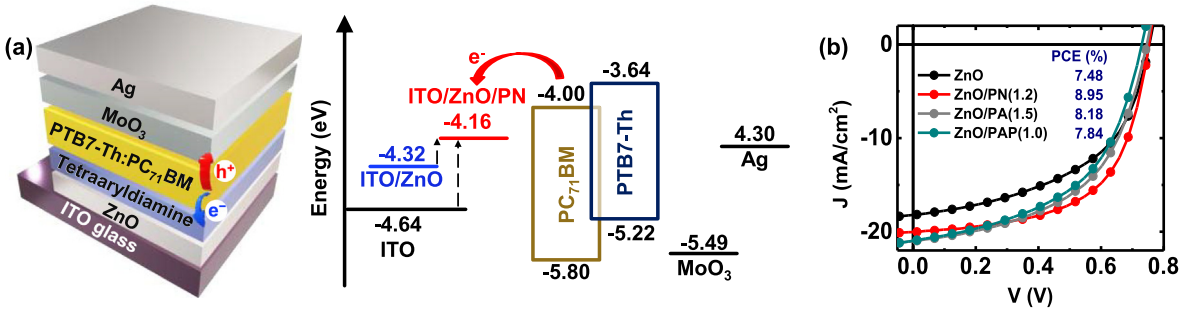

Fig. 2. (a) A schematic of PTB7-Th:$PC_{71}BM$-based organic solar cell with a tetraaryldiamine interlayer, along with the corresponding energy level diagram of the constituent layers. (b) J–V curves of devices with and without the optimized tetraaryldiamine (PN, PA, and PAP) interlayers, under simulated one sun (100 mW/cm^2).

Table 2
Photovoltaic parameters of optimal PTB7-Th:$PC_{71}BM$ devices with PN, PA, and PAP as interlayers.

ETL	V_{OC} (V)	J_{SC}^{J-V} (mA/cm^2)	J_{SC}^{EQE} (mA/cm^2)	FF (%)	PCE (%)	PCE_{max} (%)	EQE (%)	R_{se} (Ω cm^2)	R_{sh} (Ω cm^2)
ZnO	0.74 (±0.01)	17.75 (±1.09)	16.94	48.07 (±1.73)	6.34 (±0.50)	7.48	73.1	6.98 (±0.54)	179.27 (±39.63)
ZnO/PN (1.2)	0.73 (±0.02)	18.89 (±1.08)	18.55	56.45 (±2.89)	7.80 (±0.52)	8.95	77.7	5.03 (±0.95)	378.50 (±105.87)
ZnO/PA (1.5)	0.73 (±0.01)	20.51 (±0.33)	19.18	49.43 (±2.19)	7.39 (±0.49)	8.18	80.7	6.794 (±0.42)	166.76 (±36.42)
ZnO/PAP (1.0)	0.71 (±0.05)	20.64 (±0.43)	18.83	49.85 (±2.06)	7.35 (±0.80)	7.84	82.0	6.31 (±2.21)	175.47 (±23.71)

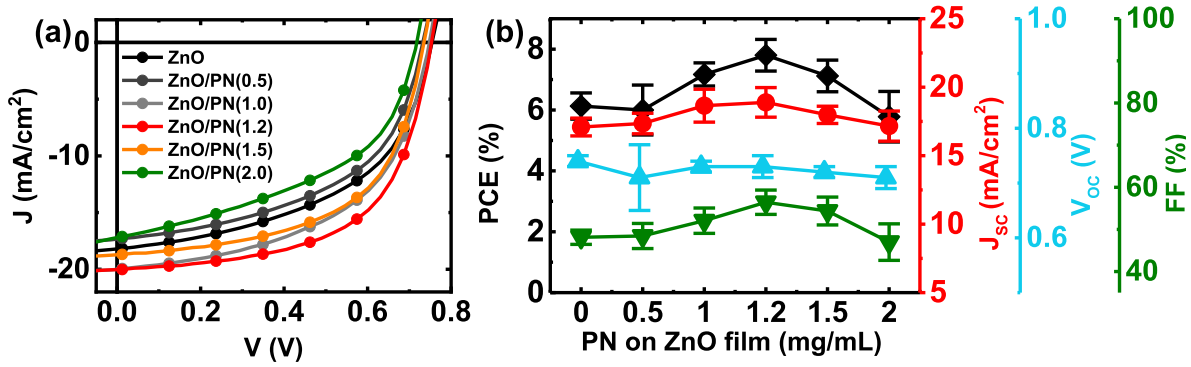

Fig. 3. Device characteristics of the solar cells with a PN interlayer deposited under different conditions: (a) J–V curves under simulated one sun. (b) Device parameters as a function of PN concentrations deposited on the ZnO film.

a maximum PCE of 7.48%, with J_{SC} of 19.93 mA/cm^2, V_{OC} of 0.73 V, and FF of 51.4%. The average PCE of the control ZnO device was 6.34% (Table 2). When a very small amount of PN was deposited on ZnO in ZnO/PN(0.5), the parameters were not affected. Interestingly, parameters like J_{SC} and FF increased appreciably for ZnO/PN (1.0) compared to those of the devices without an interlayer, while V_{OC} remained unaffected. The trends of J_{SC} and V_{OC} of the devices with interlayers agree with the previous report [43]. The highest PCE of 8.95% was achieved with ZnO/PN(1.2) with the highest V_{OC} of 0.75 V, J_{SC} of 20.03 mA/cm^2, and FF of 59.3%. The average performance parameters of the ZnO/PN(1.2) devices were 0.73 V, 18.89 mA/cm^2, 56.45%, and 7.80%, for V_{OC}, J_{SC}, FF, and PCE, respectively (Table 2). The PCE of the ZnO/PN(1.2) device was ~1.4% point higher than that of the bare ZnO device. The device performance gradually declined for ZnO/PN(1.5) with a PCE of 7.12% and for ZnO/PN(2.0) with 5.78%. J_{SC} and FF were the major factors affected by the interlayer deposition, as presented in Table S1 and Fig. 3. Similar trends of performance enhancement in devices with optimal interlayer conditions were also observed for PA and PAP (Figs. S8–S9 and Table S2). We note that device performance with an optimal interlayer was also enhanced previously for polymeric interlayers with pendant amino groups [44].

The interlayer affected the PCE of PTB7-Th:$PC_{71}BM$ devices through collection of generated charge carriers. The external quantum efficiency (EQE) was higher for the optimized tetraaryldiamine devices than for the control devices across the entire wavelength range (Fig. 4a and Fig. S9b). The peak EQE increased from 73.1% for the control to 77.7% for ZnO/PN(1.2). The EQE-based J_{SC} values for the control ZnO devices and the optimum ZnO/PN(1.2) devices were 16.94 and 18.55 mA/cm^2, respectively. The J_{SC} values from the EQE spectra were in good agreement with those from J–V measurement (Table S1). The absorption spectra of the PTB7-Th:$PC_{71}BM$ devices with and without the arylamine interlayer showed negligible differences (Fig. S10), implying that the insertion of the arylamine layer did not affect the photon flux in the solar cells [43].

The J–V curves in dark conditions showed that the optimal PN interlayer increased the rectification ratio and improved the diode characteristics (Fig. 4b). The ZnO/PN(1.2) devices had higher forward current densities and lower reverse current densities than the devices without interlayer optimization. The leakage current density of the ZnO/PN devices was significantly reduced compared to that of bare ZnO, indicating superior hole-blocking property of ZnO/PN layers [45]. Ideally, series resistance (R_{se}) should be minimized while shunt resistance (R_{sh}) should be maximized to enhance the device performance. ZnO/PN(1.2) showed more desirable R_{se} (5.03 Ω cm^2) and R_{sh} (378.50 Ω cm^2) values than the control devices (6.98 Ω cm^2 and 179.27 Ω cm^2, respectively). The small R_{se} value of ZnO/PN(1.2) suggests improved charge transport across the device, which coincides with the enhanced J_{SC} and FF. The large R_{sh} value also indicates an important reduction in leakage current of the present devices.

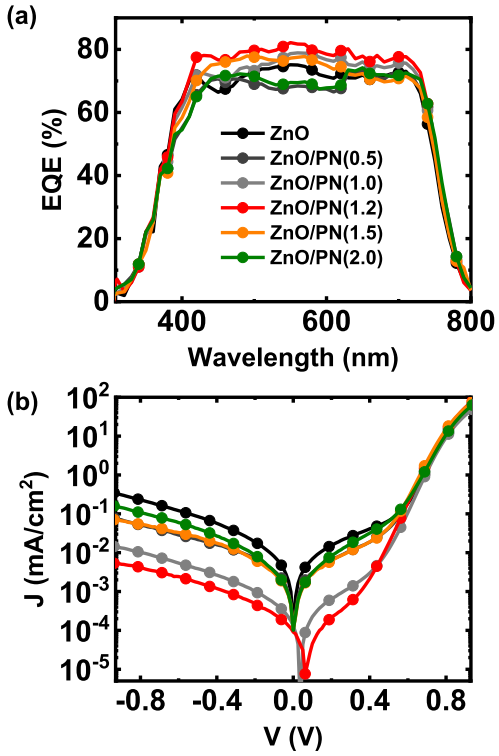

Fig. 4. (a) EQE spectra of the PTB7-Th:$PC_{71}BM$ solar cells prepared under different deposition conditions for a PN interlayer. (b) J–V curves of the devices under dark conditions.

We analyzed the impedance components of the devices and obtained Nyquist plots using EIS measurements to elucidate their charge-transport behaviors with and without the interlayer (Fig. 5a) [46]. The diameter of the semicircle represents the transport resistance of photogenerated charge-carriers. The optimal device with ZnO/PN(1.2) had a resistance of 285.8 Ω, significantly lower than that of the device with bare ZnO (1774.9 Ω). In fact, all PN-incorporated devices showed relatively lower resistances than the device with pristine ZnO, which is consistent with the

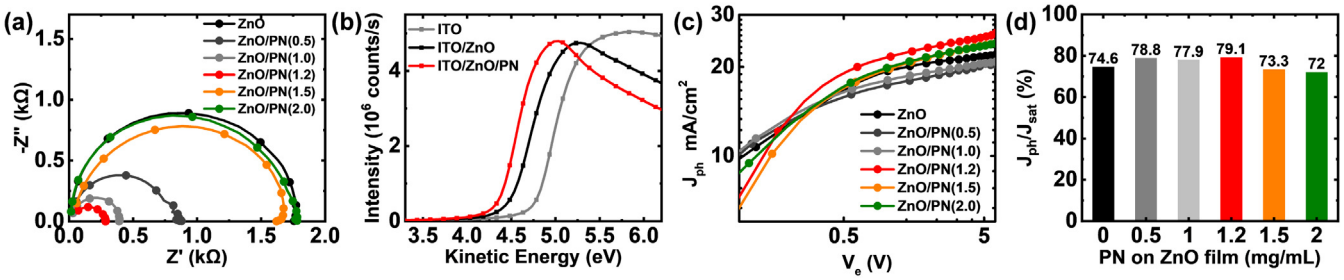

Fig. 5. (a) Nyquist plot of the solar cells with and without PN interlayers for various deposition conditions under simulated one-sun illumination. (b) UPS spectra of ITO, ITO/ZnO, and ITO/ZnO/PN(1.2). (c) J_{ph} versus V_e curves. (d) The ratio of photocurrent to saturated current density as a function of the different PN deposition conditions.

enhanced current density of the optimized devices. We also carried out UPS measurements on the ITO, ITO/ZnO, and ITO/ZnO/PN(1.2) layers to extract their work functions and further understand how the interlayer could affect charge extraction (Fig. 5b). The work function decreased from 4.64 eV for ITO to 4.32 eV for ITO/ZnO and to 4.16 eV for ITO/ZnO/PN(1.2). The work functions for ITO and ITO/ZnO are in a similar range compared to previously reported values [47,48], and The minimized value of 4.16 eV for ITO/ZnO/PN(1.2) may be attributed to an interfacial dipoles formed by the arylamine groups. The work function of ZnO/PN(1.2) could be suitable for hole blocking and electron extraction, resulting in increased J_{SC} and FF.

We also investigated the exciton dissociation properties of the control and arylamine-incorporated devices by analyzing the photocurrent density (J_{ph}), as shown in Fig. 5c,d. Here, J_{ph} was calculated as the difference between the current densities under illumination and in dark, and the effective voltage (V_e) was defined as the difference between the applied external voltage and the voltages at which J_{ph} becomes zero (V_0) [49]. The V_0 values are 0.763, 0.755, 0.763, 0.815, 0.799, and 0.750 V for the control ZnO, ZnO/PN(0.5), ZnO/PN(1.0), ZnO/PN(1.2), ZnO/PN(1.5), and ZnO/PN (2.0) devices, respectively. For all devices, J_{ph} became saturated when V_e exceeded 2 V, allowing us to extract the saturated current density (J_{sat}). Under the maximal power output conditions, J_{ph}/J_{sat} values were 74.6%, 78.8%, 77.9%, 79.1%, 73.3%, and 72.0% for the solar cells with the control ZnO, ZnO/PN(0.5), ZnO/PN(1.0), ZnO/PN(1.2), ZnO/PN(1.5), and ZnO/PN(2.0) devices, respectively. The higher J_{ph}/J_{sat} value of the devices with ZnO/PN(1.2) can be interpreted as the efficient generation and collection of free charge-carriers from the light-induced excitons.

We tracked the performance of the organic solar cells over time to analyze their stability with and without an interlayer (Fig. 6). Devices with and without arylamine interlayers were fabricated, characterized in ambient air, stored under vacuum, and tested again. Compared with the modified devices, the control devices showed more severe degradation of PCE. In contrast, interlayer-incorporated devices showed more stable operation. The devices with bare ZnO retained only about 76% of the initial PCEs, whereas the optimized ZnO/PN, ZnO/PA, and ZnO/PAP devices retained approximately 88%, 82%, and 83%, respectively, of their initial PCEs after six months. Interestingly, the FF of the devices with arylamines remained virtually constant compared with that of the devices with bare ZnO (Fig. S11). This stability enhancement may be ascribed to the passivating role of arylamines on ZnO, which prevented the degradation of the device.

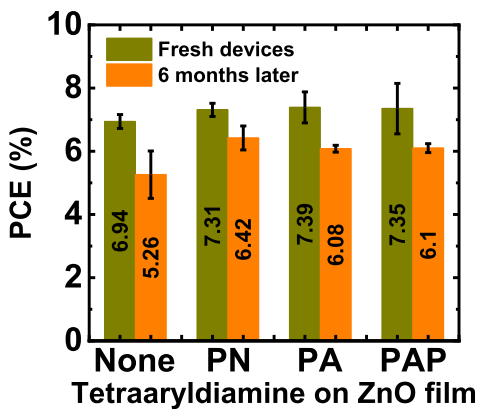

Fig. 6. PCE of the as-fabricated devices and those devices after 6 months.

Conclusions

We developed a series of new tetraaryldiamines (PN, PA, and PAP) as interlayer materials to modify the electron-transporting ZnO layer in PTB7-Th:$PC_{71}BM$ solar cells. They were synthesized by a simple and economical route and investigated through spectroscopic and thermal characterizations. All three arylamines afforded appreciable enhancements in device performance when used as an interlayer deposited onto ZnO. By varying the solution concentration during interlayer deposition, we could optimize the devices to achieve the maximum PCEs of 8.95%, 8.18%, and 7.84% for the ZnO/PN(1.2), ZnO/PA(1.5), and ZnO/PAP(1.0) devices, respectively, which were considerably higher than the PCE of the control ZnO device (7.48%). The main enhancement parameters were J_{SC} and FF. All devices with optimal tetraaryldiamine interlayers showed effective conversion of photons to electrons, as confirmed by the increased EQE. To further elucidate the mechanism of improvement by arylamines, we conducted various measurements focusing on the significance of the PN interlayer on device performance. The optimized ZnO/PN(1.2) showed a lower series resistance and superior hole-blocking properties compared to the devices with bare ZnO, as confirmed by the J–V curves and EIS, UPS, and photocurrent analysis. Furthermore, the organic solar cells with interlayers showed superior environmental stability compared to the control devices. This work offers exciting prospects for the use of simple arylamines to enhance the interfacial properties of ZnO and the performance of organic solar cells.

Declaration of Competing Interest

The authors declare that they have no known competing financial interests or personal relationships that could have appeared to influence the work reported in this paper.

Acknowledgements

This work was supported by the National Research Foundation of Korea (NRF) grant funded by the Ministry of Science and ICT of Korea (NRF-2019R1A2C1087234). This research was also funded

and conducted under "the Competency Development Program for Industry Specialists" of the Korean Ministry of Trade, Industry and Energy (MOTIE), operated by Korea Institute for Advancement of Technology (KIAT), with the project No. P0012453, Next-generation Display Expert Training Project for Innovation Process and Equipment, Materials Engineers.

Appendix A. Supplementary data

Supplementary data to this article can be found online at https://doi.org/10.1016/j.jiec.2022.06.021.

References

[1] S. Pang, Z. Wang, X. Yuan, L. Pan, W. Deng, H. Tang, et al., Angew. Chem. Int. Ed. 60 (2021) 8813.
[2] L. Ma, S. Zhang, J. Zhu, J. Wang, J. Ren, J. Zhang, et al., Nat. Commun. 12 (2021) 1.
[3] S. Bishnoi, R. Datt, S. Arya, S. Gupta, R. Gupta, W.C. Tsoi, et al., Adv. Mater. Interfaces (2022) 2101693.
[4] R. Ma, M. Zeng, Y. Li, T. Liu, Z. Luo, Y. Xu, et al., Adv. Energy Mater. 11 (2021) 2100492.
[5] A.A. Meresa, B. Parida, D.X. Long, D. Kim, T. Kim, T. Earmme, et al., Int. J. Energy Res. (2022).
[6] M. Aatif, J. Tiwari, RSC Adv. 10 (2020) 42305.
[7] F.J. Lim, A. Krishnamoorthy, G.W. Ho, ACS Appl. Mater. Interfaces 7 (2015) 12119.
[8] K. Wang, W. Li, X. Guo, Q. Zhu, Q. Fan, Q. Guo, et al., Chem. Mater. 33 (2021) 5981.
[9] X. Guo, Y. Zhang, X. Liu, S. Braun, Z. Wang, B. Li, et al., Org. Electron. 59 (2018) 15.
[10] N. Ahmad X. Zhang S. Yang D. Zhang J. Wang S. uz Zafar, Y. Li, Y. Zhang, S. Hussain, Z. Cheng, J. Mater. Chem. C 7 2019 10795.
[11] W. Lan, Y. Liu, B. Wu, B. Xu, H. Pu, B. Wei, et al., ACS Appl. Energy Mater. 2 (2019) 7385.
[12] T.K.T. Tu, S.A. Salma, M. Jeong, J.H. Kim, Y.T. Jeong, Y.-S. Gal, et al., Macromol. Res. 29 (2021) 735.
[13] W. Xu, R. Xia, T. Ye, L. Zhao, Z. Kan, Y. Mei, et al., Adv. Sci. 3 (2016) 1500245.
[14] J. Huang, Z. Xu, Y. Yang, Adv. Funct. Mater. 17 (2007) 1966.
[15] Z. He, C. Zhong, X. Huang, W.Y. Wong, H. Wu, L. Chen, et al., Adv. Mater. 23 (2011) 4636.
[16] H. Choi, H.B. Kim, S.J. Ko, J.Y. Kim, A.J. Heeger, Adv. Mater. 27 (2015) 892.
[17] L. Yan, Y. Song, Y. Zhou, B. Song, Y. Li, Org. Electron. 17 (2015) 94.
[18] S. Chen, J.R. Manders, S.-W. Tsang, F. So, J. Mater. Chem. 22 (2012) 24202.
[19] Y. Xiao, H. Wang, F. Awai, N. Shibayama, T. Kubo, H. Segawa, ACS Appl. Mater. Interfaces 13 (2021) 3969.
[20] Y. Gong, J. Zhang, B. Du, M. Wang, W.-Y. Lai, W. Huang, ACS Appl. Electron. Mater. 1 (2019) 854.
[21] W. Xu, C. Yan, Z. Kan, Y. Wang, W.-Y. Lai, W. Huang, ACS Appl. Mater. Interfaces 8 (2016) 14293.
[22] Z. Zheng, S. Zhang, J. Wang, J. Zhang, D. Zhang, Y. Zhang, et al., J. Mater. Chem. A 7 (2019) 3570.
[23] C. Wang, D. Luo, Y. Gao, G. Wang, C. Wang, P. Ma, et al., J. Phys. Chem. C 123 (2019) 16546.
[24] M. Wang, Y. Sun, J. Guo, Z. Li, C. Liu, W. Guo, Org. Electron. 74 (2019) 258.
[25] Z. Wang, Z. Wang, R. Zhang, K. Guo, Y. Wu, H. Wang, et al., Org. Electron. 76 (2020) 105458.
[26] X. Zhu, B. Guo, J. Fang, T. Zhai, Y. Wang, G. Li, et al., Org. Electron. 70 (2019) 25.
[27] J. Choi, Y. Kim, J.W. Jo, J. Kim, B. Sun, G. Walters, et al., Adv. Mater. 29 (2017) 1702350.
[28] J. Subbiah, V.D. Mitchell, N.K. Hui, D.J. Jones, W.W. Wong, Angew. Chem. Int. Ed. 56 (2017) 8431.
[29] J. Subbiah, B. Purushothaman, M. Chen, T. Qin, M. Gao, D. Vak, et al., Adv. Mater. 27 (2015) 702.
[30] R. Xia, D.S. Leem, T. Kirchartz, S. Spencer, C. Murphy, Z. He, et al., Adv. Energy Mater. 3 (2013) 718.
[31] S.A. Salma, J.H. Kim, Macromol. Res. (2022) 1.
[32] J.H. Seo, A. Gutacker, Y. Sun, H. Wu, F. Huang, Y. Cao, et al., J. Am. Chem. Soc. 133 (2011) 8416.
[33] A. Sharma, S. Singh, X. Song, D. Rosas Villalva, J. Troughton, D. Corzo, et al., Chem. Mater. 33 (2021) 8602.
[34] J. Yao, B. Qiu, Z.-G. Zhang, L. Xue, R. Wang, C. Zhang, et al., Nat. Commun. 11 (2020) 1.
[35] E. Cieplechowicz, R. Munir, M.A. Anderson, E.L. Ratcliff, G.C. Welch, ACS Appl. Mater. Interfaces 13 (2021) 49096.
[36] Y. Zhou, C. Fuentes-Hernandez, J. Shim, J. Meyer, A.J. Giordano, H. Li, et al., Science 336 (2012) 327.
[37] K.C. Kwon, H.J. Son, Y.H. Hwang, J.H. Oh, T.-W. Lee, H.W. Jang, et al., J. Phys. Chem. C 120 (2016) 1309.
[38] S.-R. Bae, T.W. Lee, K. Park, S.Y. Kim, Electron. Mater. Lett. 15 (2019) 141.
[39] T. Earmme, Y.J. Hwang, S. Subramaniyan, S.A. Jenekhe, Adv. Mater. 26 (2014) 6080.
[40] D. Fadil, R.F. Hossain, G.A. Saenz, A.B. Kaul, J. Mater. Chem. C 5 (2017) 5323.
[41] F. Neese, Wiley Interdisciplinary Rev.: Comput. Mol. Sci. 2 (2012) 73.
[42] J. Zhen, Q. Liu, X. Chen, D. Li, Q. Qiao, Y. Lu, et al., J. Mater. Chem. A 4 (2016) 8072.
[43] N. Ahmad, L. Yanxun, X. Zhang, B. Wang, Y. Zhang, H. Zhou, J. Mater. Chem. C 8 (2020) 15795.
[44] Z. Wu, C. Sun, S. Dong, X.-F. Jiang, S. Wu, H. Wu, et al., J. Am. Chem. Soc. 138 (2016) 2004.
[45] B.R. Lee, E.D. Jung, Y.S. Nam, M. Jung, J.S. Park, S. Lee, et al., Adv. Mater. 26 (2014) 494.
[46] P. Shen, M. Yao, G. Wang, R. Mi, W. Guo, Y. Bai, et al., J. Mater. Chem. A 6 (2018) 17401.
[47] H. Kang, S. Hong, J. Lee, K. Lee, Adv. Mater. 24 (2012) 3005.
[48] M. Cui, D. Li, X. Du, N. Li, Q. Rong, N. Li, et al., Adv. Mater. 32 (2020) 2002973.
[49] P.W. Blom, V.D. Mihailetchi, L.J.A. Koster, D.E. Markov, Adv. Mater. 19 (2007) 1551.